APPLICATION OF THE EULERIAN SUBGRID PROBABILITY DENSITY FUNCTION METHOD IN THE LARGE EDDY SIMULATION OF A PARTIALLY PREMIXED SWIRL FLAME

D. Fredrich*, A. J. Marquis* and W. P. Jones*
d.fredrich15@imperial.ac.uk
*Department of Mechanical Engineering, Imperial College London, London SW7 2AZ, UK

Abstract
Large Eddy Simulations (LES) of a partially premixed, swirl-stabilised flame are performed using a transported Probability Density Function (PDF) approach in combination with the Eulerian stochastic field method to account for turbulence-chemistry interaction. The corresponding subgrid scale (sgs) stresses and scalar fluxes are modelled using a dynamic version of the Smagorinsky model and a gradient diffusion approximation, respectively. A 15-step reduced methane (CH_4) mechanism containing 19 species is employed for the description of all chemical reactions. The test case involves a widely studied gas turbine model combustor with complex geometry. Simulations are carried out for two combustor operating conditions utilising both one and four stochastic fields. The overall velocity, temperature and major species mass fraction results as well as the instantaneous thermochemical properties are shown to be in good agreement with experimental measurement data demonstrating the capabilities of the employed LES method.

Introduction
The highly turbulent behaviour of swirl-stabilised flames involving fast chemical reactions and sophisticated geometrical features strongly limits the contemporary understanding of the complex flow physics encountered in modern gas turbine combustors. A potentially powerful numerical tool capable of providing better insight into some of the physical processes associated with turbulent reacting flow is Large Eddy Simulation (LES). The concept behind LES methods is the direct computation of large-scale, energetic turbulent motions while the effects of motions whose 'size' is smaller than a defined filter width are modelled. One of the main challenges in the development of such methods for turbulent combustion is the interaction between turbulence and chemistry on the small, unresolved subfilter - or subgrid - scales (sgs). These so-called turbulence-chemistry interactions are governed by highly non-linear chemical reaction rates and appear in the form of a filtered source term in the LES scalar equations requiring extensive modelling work. Various combustion models addressing the closure problem have been proposed in the past, though most of them formulated for one specific flame regime only. An overview of the different modelling techniques can be found, amongst others, in a review by Pitsch [1].

The subgrid combustion model underlying this work is based on a transported Probability Density Function (PDF) approach solved by the Eulerian stochastic field method. It comes with the advantage of a regime independent description of turbulent flames, which becomes particularly useful in the context of gas turbine combustion. State of the art gas turbine combustors are designed to operate under lean partially premixed conditions in order to effectively reduce pollutant emissions such as nitrogen oxides (NO_x) and carbon monoxide (CO). In the partially premixed flame regime, parts of the flow field are governed by premixed flame propagation and finite-rate effects, i.e. auto-ignition, extinction or ignition, while other parts will display mixing

controlled reactions as encountered in diffusion (non-premixed) flames. It has been shown in the past [2–4] that it is possible to capture these phenomena within a single LES framework by introducing the present fully Eulerian subgrid PDF approach to account for turbulence-chemistry interaction. The method has since been successfully applied to a wide range of flow configurations and was recently extended to stratified [5] and spray [6, 7] combustion. In a rigorous study of an industrial gas turbine combustor, Bulat et al. [8, 9] applied the method to a lean, partially premixed flame achieving good reproduction of the measured flow statistics. Local extinction of the flame was shown to be due to turbulence-chemistry effects rather than large-scale mixing and the combustor was found to have regions of diffusion flame regimes. Furthermore, it was found that the inclusion of radiative heat transfer has a noticeable influence on the flame location and leads to an improved prediction of the temperature field and species distribution.

Another widely studied test case providing a solid basis for the validation of LES combustion models is the so-called PRECCINSTA (Prediction and Control of Combustion Instabilities in Industrial Gas Turbines) burner. The gas turbine model combustor was experimentally investigated by Meier et al. [10] and has been the focus of a number of numerical simulations [11–16]. Comparisons between experiments and LES were first reported by Galpin et al. [12] whose simulations predicted slightly faster combustion - manifesting itself in a shortened flame length - and overestimated temperatures in the Outer Recirculation Zone (ORZ). The latter was attributed to the assumption of adiabatic combustion chamber walls, which preclude the replication of any heat loss occurring in the experiments. These findings were later confirmed in ensuing LES studies by different authors coming to similar conclusions. Franzelli et al. [14] underlined the importance of resolving the fuel injection, as opposed to prescribing a perfectly premixed mixture at the domain inlet, in order to obtain better agreement between the simulated and measured statistical quantities especially in terms of RMS values. Note that all of the above-cited numerical studies were performed using either simple chemistry involving very few species and reaction steps or tabulated chemistry based on fully premixed, laminar flame calculations.

In this work, the flame regime independent Eulerian subgrid PDF approach with reduced chemistry involving 19 species is applied to the PRECCINSTA model combustor. The objective is to assess the predictive capabilities of the employed LES method in the context of partially premixed combustion in a complex geometry. For this purpose, test cases for two different combustor operating conditions are simulated and results are compared against available experimental data. This includes characterisation of the flow field using mean axial and radial velocity component profiles at different locations in the combustion chamber as well as a description of the flame based on both mean and Root Mean Square (RMS) temperature, carbon dioxide (CO_2) and methane (CH_4) profiles. The simulated mean and instantaneous flame structure is further assessed in a qualitative comparison with experimental hydroxide (OH) images. Finally, the representation of fundamental thermochemical properties is evaluated by analysis of the instantaneous temperature-mixture fraction relation.

Mathematical formulation

In LES the separation of large- and small-scale turbulent motions is achieved through a spatial filtering operation over the entire flow domain Ω. The spatial filter of a function $f = f(\mathbf{x}, t)$ is defined as its convolution with a filter function G according to:

$$\overline{f}(\mathbf{x}, t) = \int_{\Omega} G(\mathbf{x} - \mathbf{x}'; \Delta(\mathbf{x})) f(\mathbf{x}', t) \mathrm{d}\mathbf{x}' \tag{1}$$

where the filter width Δ is taken to be the cube root of the local grid cell volume. In order to account for the strong density variations arising in combusting flows, additional density weighted

- or Favre - filtering defined by $\widetilde{f} = \overline{\rho f}/\overline{\rho}$ can be introduced. Application of this filter to the equations of motion, i.e. mass conservation (2) and momentum conservation (3), and to the scalar transport equations (4) results in the following set of filtered equations:

$$\frac{\partial \overline{\rho}}{\partial t} + \frac{\partial \overline{\rho}\widetilde{u}_i}{\partial x_i} = 0 \tag{2}$$

$$\frac{\partial \overline{\rho}\widetilde{u}_i}{\partial t} + \frac{\partial \overline{\rho}\widetilde{u}_i\widetilde{u}_j}{\partial x_j} = -\frac{\partial \overline{p}}{\partial x_i} + \frac{\partial}{\partial x_j}\left(2\mu\widetilde{S}_{ij}\right) - \frac{\partial \tau_{ij}^{sgs}}{\partial x_j} \tag{3}$$

$$\frac{\partial \overline{\rho}\widetilde{\phi}_\alpha}{\partial t} + \frac{\partial \overline{\rho}\widetilde{u}_j\widetilde{\phi}_\alpha}{\partial x_j} = \frac{\partial}{\partial x_j}\left(\frac{\overline{\mu}}{\sigma}\frac{\partial \widetilde{\phi}_\alpha}{\partial x_j}\right) - \frac{\partial J_{\alpha,j}^{sgs}}{\partial x_j} + \overline{\rho\dot{\omega}}_\alpha \tag{4}$$

The subgrid scale stress tensor $\tau_{ij}^{sgs} = \overline{\rho}\left(\widetilde{u_i u_j} - \widetilde{u}_i\widetilde{u}_j\right)$ is determined via the Smagorinsky model [17], which introduces a subgrid scale viscosity μ_{sgs} to mimic the diffusion process on the dissipative small-scales:

$$\mu_{sgs} = \overline{\rho}(C_s\Delta)^2||\widetilde{S}_{ij}|| \tag{5}$$

where $\widetilde{S}_{ij} = \frac{1}{2}\left(\frac{\partial \widetilde{u}_i}{\partial x_j} + \frac{\partial \widetilde{u}_j}{\partial x_i}\right)$ and $||\widetilde{S}_{ij}|| \equiv \sqrt{2\widetilde{S}_{ij}\widetilde{S}_{ij}}$ are the resolved rate of strain tensor and its respective Frobenius norm. The Smagorinsky parameter C_s is obtained through the dynamic procedure of Piomelli and Liu [18]. The isotropic part of the viscous and subgrid scale stresses is absorbed into the pressure. Based on a Lewis number unity assumption, the scalar transport equations (4) are expressed in terms of a general scalar $\phi_\alpha = [\phi_1, ..., \phi_{N_{sc}}]$ representing the species mass fractions Y_α and the enthalpy h where N_{sc} is the number of scalars required to describe the system, i.e. species plus enthalpy. A low-Mach-number flow, constant thermodynamic pressure and equal diffusivities for all species $D_\alpha = D$, which can be related to the viscosity via the Prandtl - or Schmidt - number $\sigma = \mu/\rho D$, have been assumed in the formulation. A gradient diffusion approximation is adopted for the scalar fluxes $J_{\alpha,j}^{sgs}$ [19]. The filtered chemical source term representing the net rate of species formation through chemical reaction $\overline{\rho\dot{\omega}}_\alpha$ remains unclosed and requires modelling.

The combustion model underlying the present work is a fully Eulerian transported subgrid PDF approach. Following Gao and O'Brien [20] and through the application of Favre filtering, a joint subgrid PDF can be derived according to:

$$\widetilde{P}_{sgs}(\underline{\psi}; \mathbf{x}, t) = \frac{1}{\overline{\rho}}\int_\Omega \rho G(\mathbf{x} - \mathbf{x}', \Delta(\mathbf{x}))\mathscr{F}(\underline{\psi}; \mathbf{x}', t)\mathrm{d}\mathbf{x}' \tag{6}$$

Here, $\mathscr{F}$ denotes the joint PDF, which is the product of the fine-grained probability density function P_α of each reactive scalar:

$$\mathscr{F}(\underline{\psi}; \mathbf{x}, t) = \prod_{\alpha=1}^{N_s} P_\alpha = \prod_{\alpha=1}^{N_s} \delta\left[\psi_\alpha - \phi_\alpha(\mathbf{x}, t)\right] \tag{7}$$

where ψ_α is the sample - or composition - space of the reactive scalar ϕ_α and δ is the Dirac-function. An exact equation describing the evolution of $\widetilde{P}_{sgs}$ can be derived from the appropriate conservation equations using standard methods, e.g. [20]. This formulation contains the chemical reaction term (I), which appears in closed form, as well as two additional unknown terms representing subgrid scale convection (II) and molecular diffusion (III) of the PDF. In the present work, these unknown terms are approximated, respectively, by a gradient closure directly analogous to the LES Smagorinsky model and by the Linear Mean Square Estimation

(LMSE) closure [21]. Taking into account the approach of Brauner et al. [5], the subgrid PDF evolution equation appears in its final form:

$$\overline{\rho}\frac{\partial \widetilde{P}_{sgs}(\underline{\psi})}{\partial t} + \overline{\rho}\widetilde{u}_j\frac{\partial \widetilde{P}_{sgs}(\underline{\psi})}{\partial x_j} = \underbrace{\sum_{\alpha=1}^{N_s}\frac{\partial}{\partial \psi_\alpha}\left[\overline{\rho}\dot{\omega}_\alpha(\underline{\psi})\widetilde{P}_{sgs}(\underline{\psi})\right]}_{\textbf{I:}\ \text{closed chemical reaction term}}$$
$$\underbrace{+\frac{\partial}{\partial x_j}\left[\left(\frac{\mu}{\sigma}+\frac{\mu_{sgs}}{\sigma_{sgs}}\right)\frac{\partial \widetilde{P}_{sgs}(\underline{\psi})}{\partial x_j}\right]}_{\textbf{II:}\ \text{sgs convection term (gradient closure)}} \underbrace{-\frac{C_d}{2\tau_{sgs}}\sum_{\alpha=1}^{N_s}\frac{\partial}{\partial \psi_\alpha}\left[\overline{\rho}(\psi_\alpha-\widetilde{\phi}_\alpha(\mathbf{x},t))\widetilde{P}_{sgs}(\underline{\psi})\right]}_{\textbf{III:}\ \text{molecular diffusion term (LMSE closure)}} \tag{8}$$

Here, the values 0.7 and 2.0 are assigned to the subgrid scale - or turbulent - Schmidt number σ_{sgs} and the micro-mixing constant C_d, respectively. The micro-mixing time scale τ_{sgs} is assumed to be given by:

$$\tau_{sgs} = \frac{\overline{\rho}\Delta^2}{\mu_{sgs}}\left(1-\exp\left(-\mathscr{R}^2\right)\right) \tag{9}$$

with a subgrid scale turbulence Reynolds number defined as $\mathscr{R} = \mu_{sgs}/\mu$. The closed form of the subgrid PDF evolution equation (8) is solved using the Eulerian stochastic field method, where $\widetilde{P}_{sgs}(\underline{\psi})$ is represented by an ensemble of N stochastic fields - namely $\xi_\alpha^n(\mathbf{x},t)$ - for each of the N_s reactive scalars. The joint subgrid PDF equation (6) can then be rewritten as follows:

$$\widetilde{P}_{sgs}(\underline{\psi};\mathbf{x},t) = \frac{1}{N}\sum_{n=1}^{N}\frac{1}{\overline{\rho}}\int_\Omega \rho G(\mathbf{x}-\mathbf{x}',\Delta(\mathbf{x}))\times\prod_{\alpha=1}^{N_s}\delta\left[\psi_\alpha-\xi_\alpha^n(\mathbf{x},t)\right]\mathrm{d}\mathbf{x}' \tag{10}$$

Two approaches by Valiño [22] and Sabel'nikov [23] exist for the derivation of a system of stochastic differential equations equivalent to the subgrid PDF evolution equation (8). In the present work, the Itô formulation is adopted for the stochastic integral [22] and the stochastic fields thus evolve according to:

$$\begin{aligned}\overline{\rho}\mathrm{d}\xi_\alpha^n + \overline{\rho}\widetilde{u}_i\frac{\partial \xi_\alpha^n}{\partial x_i}\mathrm{d}t = \overline{\rho}\dot{\omega}_\alpha^n(\underline{\xi}^n)\mathrm{d}t + \frac{\partial}{\partial x_i}\left[\Gamma'\frac{\partial \xi_\alpha^n}{\partial x_i}\right]\mathrm{d}t \\ - \frac{C_d\overline{\rho}}{2\tau_{sgs}}\left(\xi_\alpha^n-\widetilde{\phi}_\alpha\right)\mathrm{d}t + \sqrt{2\overline{\rho}\frac{\mu_{sgs}}{\sigma_{sgs}}}\frac{\partial \xi_\alpha^n}{\partial x_i}\mathrm{d}W_i^n\end{aligned} \tag{11}$$

where $\Gamma' = \frac{\mu}{\sigma}+\frac{\mu_{sgs}}{\sigma_{sgs}}$ is the total diffusion coefficient. The Wiener process $\mathrm{d}W_i^n$ is approximated by time-step increments $\eta_i^n\sqrt{\mathrm{d}t}$ where η_i^n is a $\{-1,1\}$ dichotomic random vector, different for each field but independent of the spatial location $\mathbf{x}$. The Favre filtered value of each reactive scalar ϕ_α can finally be obtained from averaging over the stochastic fields:

$$\widetilde{\phi}_\alpha = \frac{1}{N}\sum_{n=1}^{N}\xi_\alpha^n \tag{12}$$

Test case

The PRECCINSTA gas turbine model combustor considered in this work was initially the scope of an experimental test campaign conducted by Meier et al. [10] at the DLR (German Aerospace Center). Measurements were performed for three different operating conditions by varying the fuel mass flow rate to adjust the global equivalence ratio Φ_{glob} of the mixture. An oscillating

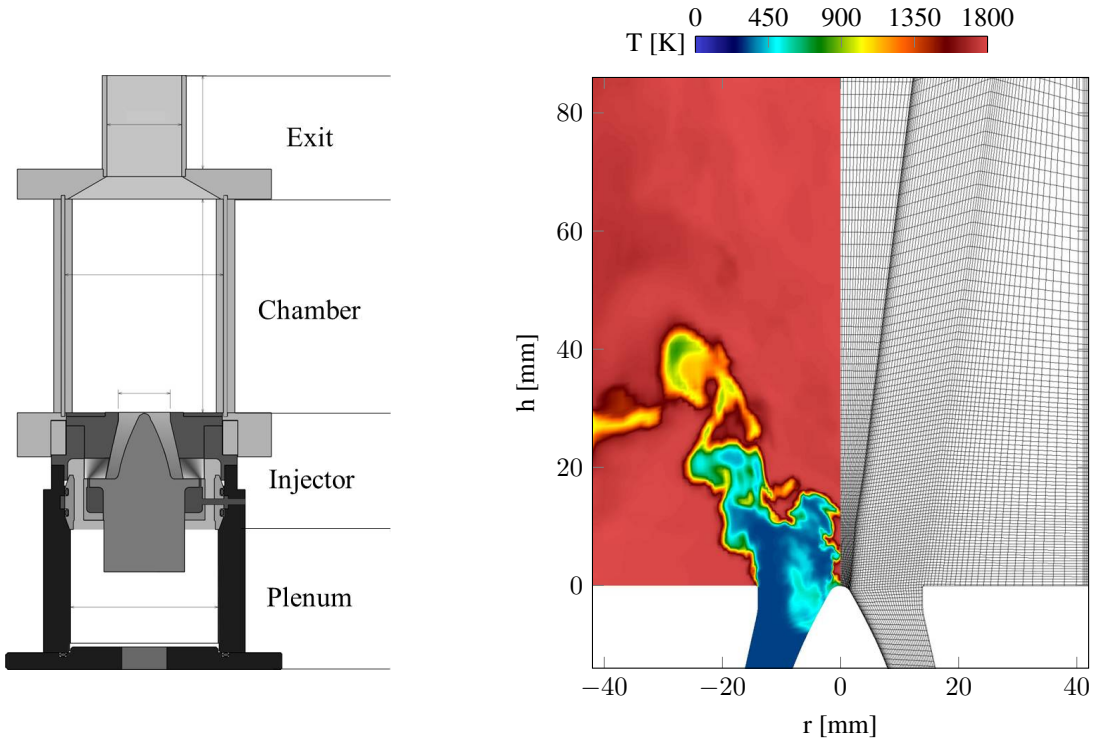


Figure 1. Schematic [10] of the PRECCINSTA combustor (left) and snapshot of an instantaneous LES temperature field with a close-up of the computational mesh (right).

flame undergoing self-excited thermo-acoustic instabilities was observed at Φ_{glob} = 0.7 (case 1). Increasing the fuel mass flow rate to Φ_{glob} = 0.83 (case 2a) resulted in a 'quiet' flame not exhibiting any oscillations whereas Φ_{glob} = 0.75 (case 2b) produced a subtly pulsating flame. The combustor geometry is schematically depicted in Fig. 1 and comprises four sections. Dry, pure air at atmospheric conditions is fed into the first section (plenum) through a large orifice. The second section (injector) consists of a radial swirler followed by a 'bluff body' and was derived from an industrial design by Turbomeca. In between each of the 12 swirler vanes, methane is injected into the air stream through a 1 mm diameter fuel hole with high momentum to ensure good mixing. The resulting mixture swirls around the 'bluff body' before entering the third section (chamber). The combustion chamber is made of 1.5 mm thick quartz glass windows with a 85 x 85 mm^2 cross section area and a total length of 114 mm. Its entry plane - aligned with the 'bluff body' tip - is defined as axial location h_0 = 0 mm for all measurements. The burnt combustion products exit the domain through the fourth section (exit) connecting the combustor to the atmosphere via a converging duct. Comprehensive experimental data is available from Laser Doppler Velocimetry (LDV) measurements for the cases 1 and 2b as well

Table 1. Systematic and statistical uncertainties of selected quantities in the experimental measurements [10].

Uncertainty	Velocity	Temperature	Mixture fraction	Mass fraction	
				CH_4	CO_2
Systematic	<0.5%	±3-4%	±3-4%	+5-9%	±3-5%
Statistical	±1.5-2%	±2.5%	±1%	±1-3%	±7%

as laser Raman scattering measurements for the cases 1 and 2a. These provide both mean and RMS values of the velocity, temperature, mixture fraction and major species mass fractions. Measurements were performed along radial profiles in one vertical plane at different axial locations within the combustion chamber. Additional planar Laser-Induced Fluorescence (LIF) of OH radicals was applied to visualise the flame structure. The experimental systematic and statistical measurement uncertainties are presented in Table 1.

The in-house, block-structured, boundary conforming coordinate LES code BOFFIN-LES is employed to carry out the computations. It is fully parallelised by means of domain decomposition and MPI message passing routines. The code utilises a second-order-accurate finite volume method, based on a low-Mach-number, pressure based, variable density formulation. For the momentum equation convection terms, an energy-conserving discretisation scheme is used. All other spatial derivatives are discretised with second-order central differences, with the exception of the convective terms in the scalar equations. These are discretised using a Total Variation Diminishing (TVD) scheme to avoid unphysical overshoots. A description of the weak first-order temporal approximation used for solving the stochastic field equations can be found in [24]. Test cases 1 and 2a corresponding to an oscillating flame (Φ_{glob} = 0.7) and a 'quiet' flame (Φ_{glob} = 0.83) are considered in this work. Both one and four stochastic fields are utilised to represent the influence of the subgrid scale contributions. However, due to limited computational resources all mean statistics were collected using one stochastic field only. The computational domain is almsot identical to the combustor geometry investigated in the experimental test campaign. A close-up of the generated block-structured mesh containing $\sim$2.7 million cells is shown on the right-hand side of Fig. 1. In order to account for preheating of the mixture, as observed in the experiments [10], both air and methane are injected at a temperature of 320 K and a pressure of 1 bar. The inlet velocities have been adjusted accordingly to reflect the prescribed mass flow rates. A zero-gradient pressure boundary condition is adopted for the outlet plane and all domain walls are treated as adiabatic. Radiative heat transfer is included in the simulations through the radiation model described in [25]. The chemistry is represented by a 15-step Augmented Reduced Mechanism (ARM) involving 19 species, which was derived by Sung et al. [26] from the full GRI 3.0 mechanism.

Results and discussion

Results for the 'quiet' flame (Φ_{glob} = 0.83) are presented and discussed first. In order to get a better idea of the flame topology, mean and instantaneous images of the OH intensity are displayed in Fig. 2 in a strictly qualitative comparison between experiments and simulation. Generally, the LES does a good job of replicating the flame structure despite not being able to resolve the smallest turbulent length scales captured by the LIF measurements. Wrinkling of the flame front seems to increase with downstream position where most of the smaller structures are found. The flame's characteristic V-shape can be clearly identified in both studies although mismatching spreading angles of the outer flame surface lead to a reduced flame width in the simulation. An over predicted degree of premixing (described later based on Fig. 5) could potentially be a cause for the underestmated outer flame angle as it tends to increase the burning rate [12]. Finally, a noticeable difference in the depicted flame lengths can be determined from the mean images. The jet of low OH intensities in the experimental image extends beyond 30 mm into the combustion chamber whereas reaching only about 25 mm in the LES snapshot.

Figure 3 shows radial profiles of the mean and RMS temperature and CH_4 mass fraction at five different axial positions in the combustion chamber. High mean temperatures near the centreline characterise the Inner Recirculation Zone (IRZ) where burnt gases are transported back to the flame front with the purpose of stabilising the flame. These temperatures, both

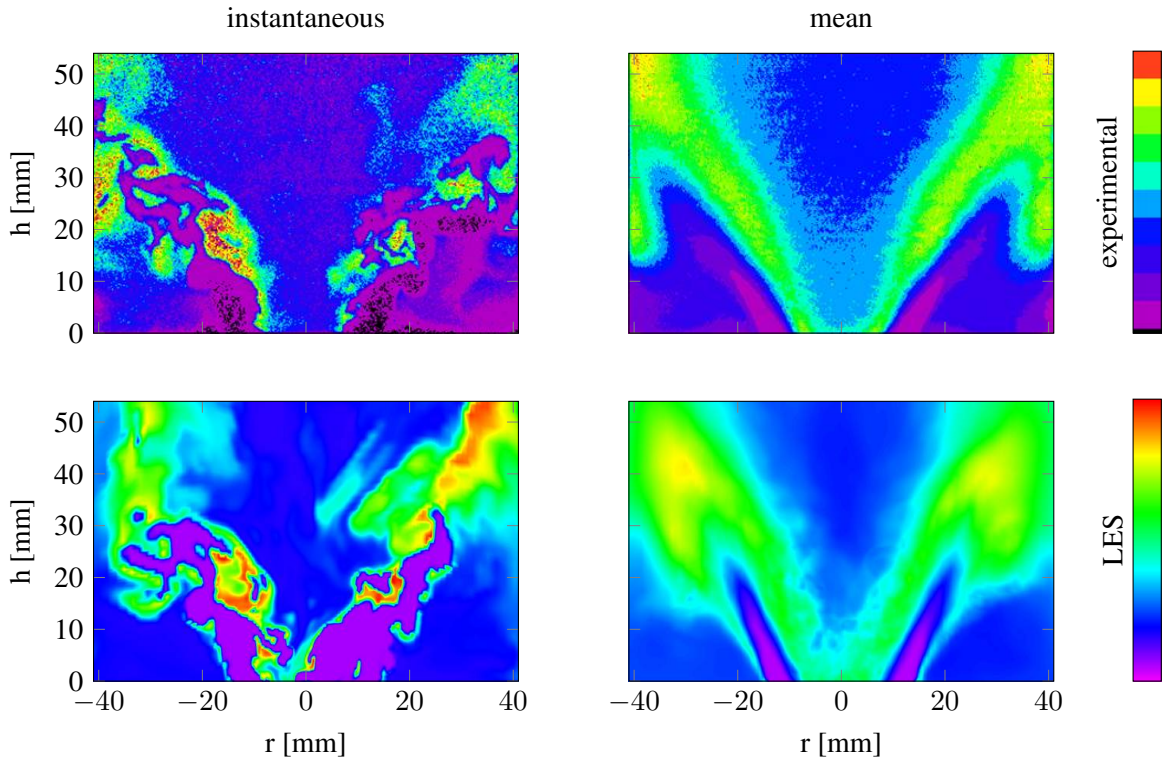


Figure 2. Comparison of the instantaneous (left) and mean (right) flame structure based on experimental OH-LIF measurements (top) and LES snapshots of the OH mass fraction (bottom). Note that the LES colour scale had to be approximated since the measurements are qualitative only.

mean and RMS, as well as the CH_4 mass fractions in this region are in excellent agreement with experimental data. Discrepancies between the measured and simulated temperature profiles appear towards the combustion chamber walls as a result of two overlapping effects. Heat loss occuring in the experimental test campaign, also mentioned in e.g. [13], can be determined by cross-correlating the temperature and CH_4 mass fraction profiles at axial positions h_6 and h_{10}. In the region $r > 25$ mm, both the computed and measured mean and RMS values of the CH_4 mass fraction are approximately zero indicating a fully burnt mixture. The temperature deviation in this region is therefore most likely caused by experimental heat loss. Further downstream at h_{20} and h_{30}, the temperature differences become more significant and are complemented by a discrepancy in the CH_4 mass fraction profiles. Compared to measurement data, an earlier consumption of CH_4 - with downstream position - occurs and the mean temperatures converge towards their 'equilibrium' state at a quicker rate. A shortened flame length can be concluded, as already observed in the OH images (Fig. 2), corresponding to faster combustion, which was first described by Galpin et al. [12]. The limitation of utilising only one stochastic field in the calculation of the subgrid PDF evolution equation may be identified as a potential cause for this. Previous findings [2, 24] suggest that eight stochastic fields provide a reasonable compromise between prediction accuracy and computational costs. In accordance with the under predicted flame length, RMS temperature and CH_4 mass fraction intensities towards the combustion chamber walls are not sufficiently captured by the LES particularly at the downstream positions. Nevertheless, a fair description of the general RMS trends can be observed.

A simulation of the oscillating flame case ($\Phi_{glob} = 0.7$) was performed to complement the 'quiet' flame results presented above. Note that the low-Mach-number solver applied in this

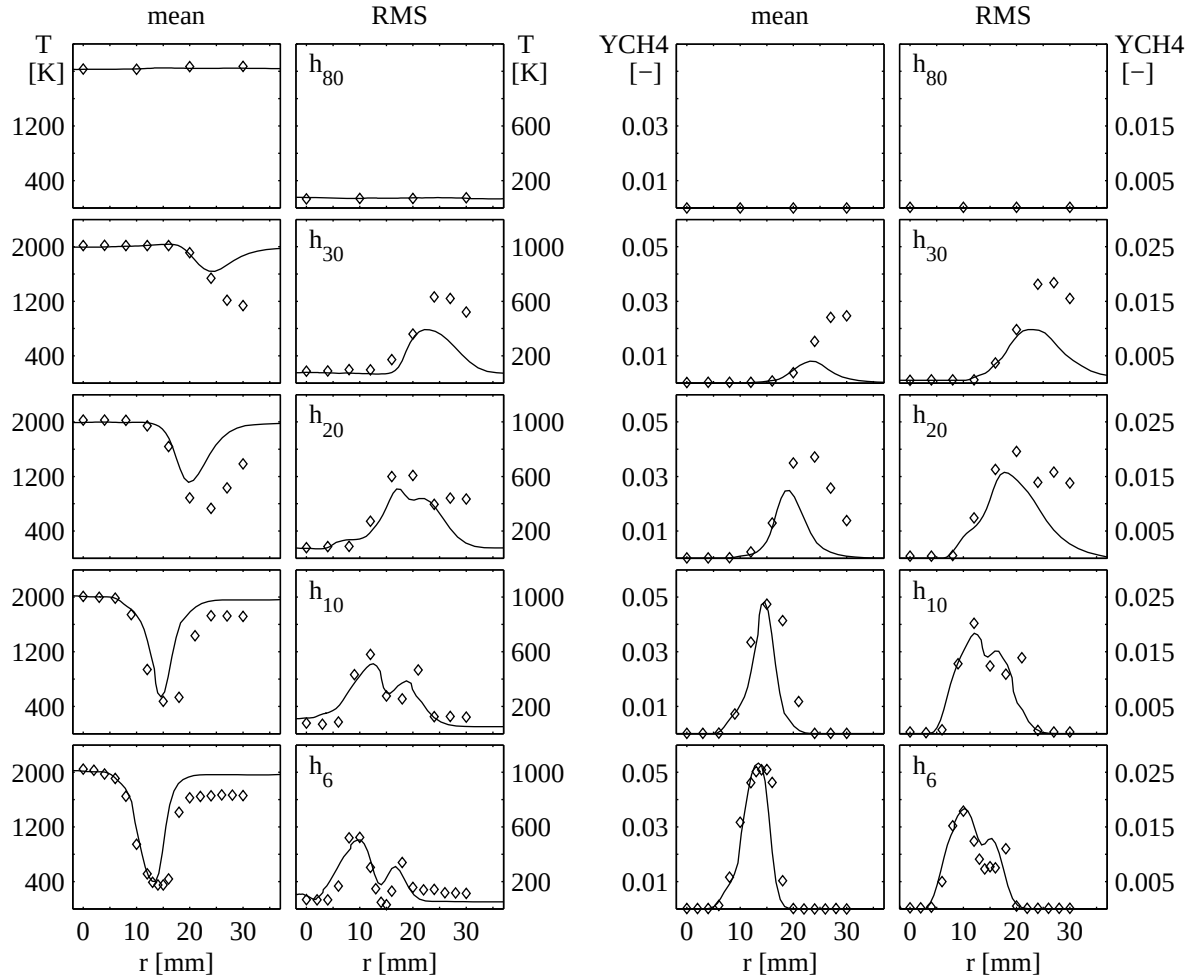


Figure 3. Radial profiles of both the mean and RMS temperature (left) and CH_4 mass fraction (right) for the 'quiet' flame case obtained from experiments ($\diamond$) and LES ($-$) at axial locations h = 6, 10, 20, 30, 80 mm.

work will not propagate acoustic waves, prohibiting the reproduction of thermo-acoustic instabilities observed in the experiments [10]. Radial profiles of the mean axial and radial velocity component for the 'oscillating' flame are shown on the left-hand side of Fig. 4. When characterising the flow field, three distinctive flow regions can be identified. An Inner Recirculation Zone (IRZ), created by the swirling flow to stabilise the flame, can easily be detected due to the high negative velocities around the combustor centreline. The conically shaped, swirling jet of unburnt gases is characterised by high axial velocities peaking at 40 m/s and high radial velocity magnitudes reaching approximately 20 m/s. Lower velocities towards the combustion chamber walls indicate the transition into an Outer Recirculation Zone (ORZ), which is located outside of the experimentally measured region. With increasing downstream position, the high velocity jet widens and shifts towards the combustion chamber walls reducing the size of the ORZ while widening the IRZ. All of the above-mentioned flow characteristics are captured in the simulation and the quantitative velocity results match experimental data with very high accuracy.

The right-hand side of Fig. 4 presents radial profiles of the mean and RMS temperature. A corresponding instantaneous snapshot of the temperature field is depicted in Fig. 1 illustrating the highly turbulent flame behaviour. Looking at the mean profiles, general temperature

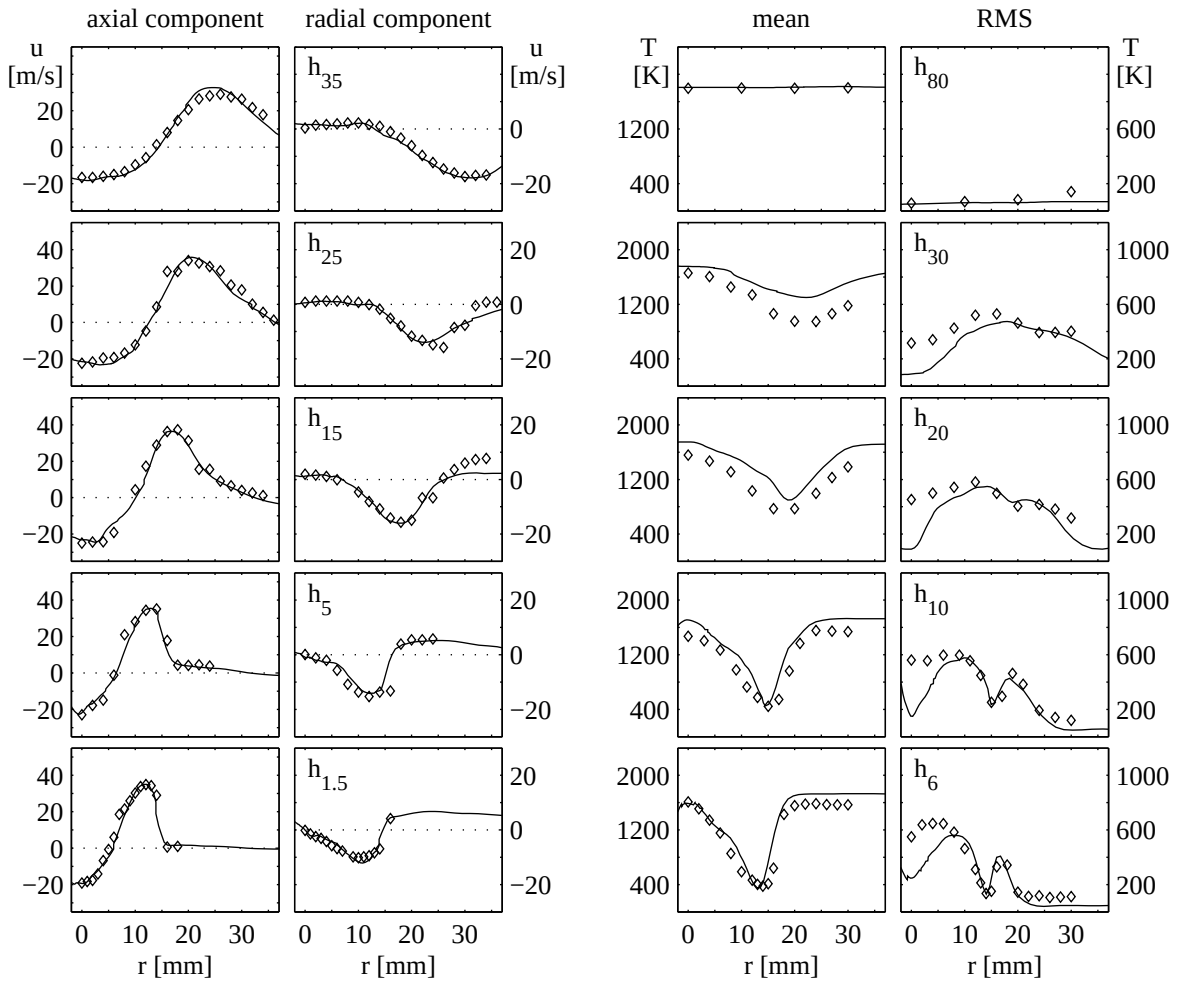


Figure 4. Radial profiles of the mean axial and radial velocity component (left) and the mean and RMS temperature (right) for the oscillating flame case obtained from experiments (◇) and LES (−) at axial locations h = 6, 10, 20, 30, 80 mm.

trends including the location of the temperature dip representing unburnt gases are well reproduced by the LES. Unaccounted for heat loss effects at the combustion chamber walls as well as a shortened flame length can be detected similar to the 'quiet' flame case. At h_{80} both the experimental and numerical temperatures reach a homogeneous 'equlibrium' state at the adiabatic flame temperature of just over 1800 K. From the RMS profiles, it becomes clear that temperature fluctuations are consistently underestimated towards the combustor centreline. The method's incapabilty to reproduce an oscillating flame undergoing self-excited thermo-acoustic instabilities serves as a possible explanation for the underestimation. In a previous LES of the same combustor, Franzelli et al. [14] have shown a significant improvement of RMS temperature results close to the centreline by resolving flame oscillation. Despite this shortcoming, RMS temperature profiles away from the centreline are accurately reproduced. Radial profiles of the mean and RMS CO_2 mass fraction, depicted on the left-hand side of Fig. 5, show very similar trends supporting the aforementioned findings.

The numerically predicted thermochemistry can be analysed in terms of the instantaneous relation between temperature and mixture fraction as visualised on the right-hand side of Fig. 5 for four axial locations. Each experimental scatter represents one single-shot laser Raman scattering measurement taken at different radial positions over time. All LES scatters were obtained

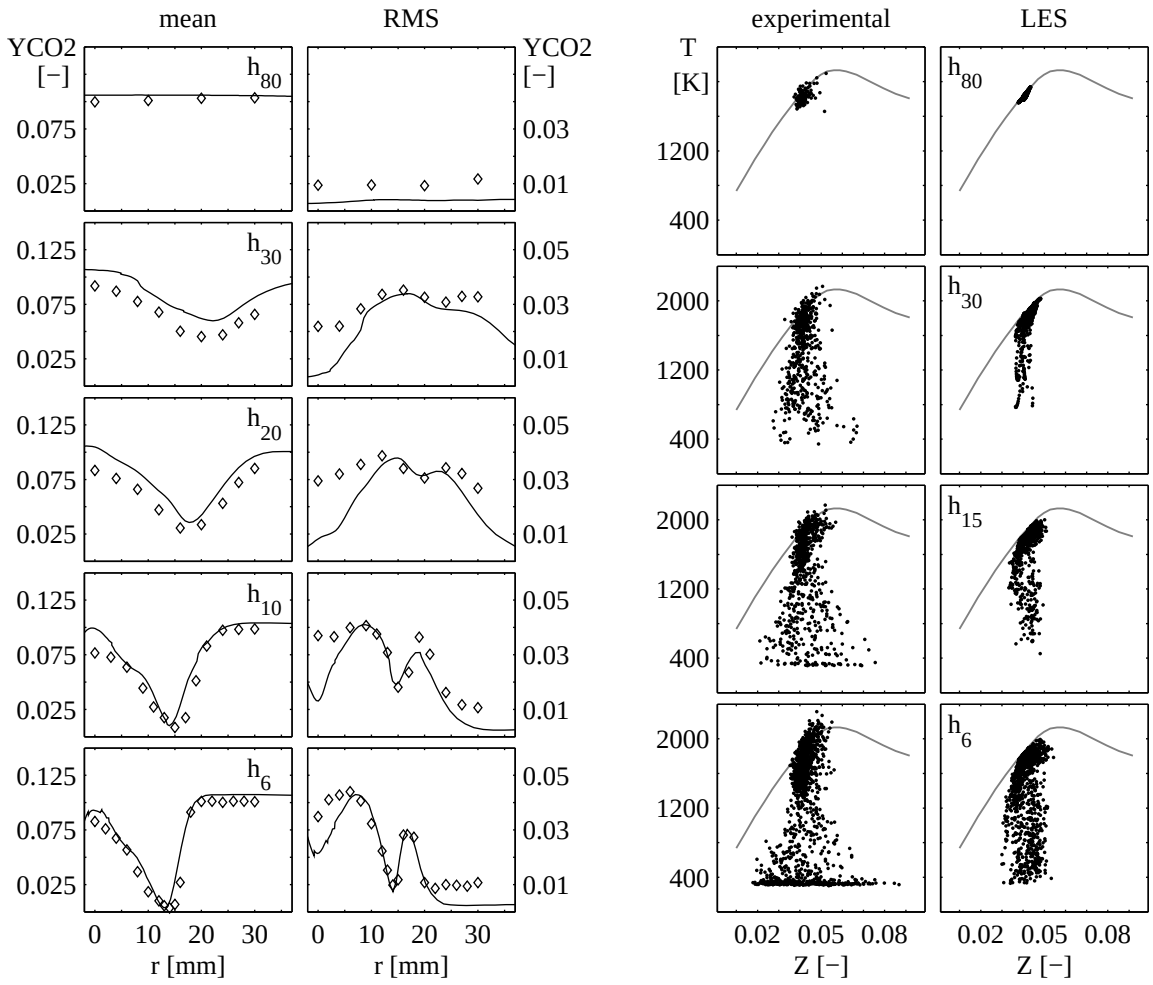


Figure 5. Radial profiles of the mean and RMS CO_2 mass fraction obtained from experiments ($\diamond$) and LES ($-$) (left). Experimental and LES scatter plots of the instantaneous temperature versus mixture fraction (right). Results are shown for the oscillating flame case at axial locations h = 6, 10, 15, 20, 30, 80 mm.

at identical locations in the chamber using an additional simulation with four stochastic fields on a coarser mesh ($\sim$0.5 million cells). A solid line indicates the adiabatic flame temperature and the global mixture fraction is $Z_{glob} = 0.0391$. The temperature distribution at h_6 suggests that the assumed inlet temperature of 320 K is suitable to recreate experimental preheating of the mixture. Looking at the evolution of the simulated temperature-mixture fraction distribution with downstream location, the shortened flame length determined in the mean temperature and CO_2 mass fraction results can be observed once again. Unlike the experimental findings at axial position h_6, only a small amount of scatters is still located within the fresh gas region below approximately 400 K. Furthermore, at h_{15}, all of the scatters have moved up into either the reaction zone with intermediate temperatures or the fully burnt region close to the theoretical adiabatic flame temperature. In terms of the mixture fraction distributions, experimental extreme values of about $Z_{min} \approx 0.015$ and $Z_{max} \approx 0.08$ can be observed. It becomes clear that the LES does not reproduce such a wide range of mixture fraction values but instead predicts a higher degree of premixing. The expanded experimental distribution is likely to be caused by the occurrence of thermo-acoustic instabilities periodically varying the amount of fuel in the mixture, as observed experimentally by Meier et al. [10] and numerically by Franzelli et al. [14]. Overall, the

computed instantaneous temperature-mixture fraction relation matches the experimental results including a reasonably estimated mixture fraction distribution.

Conclusions

The PRECCINSTA gas turbine model combustor was simulated for two different operating conditions using LES in conjunction with the Eulerian subgrid PDF combustion model accounting for turbulence-chemistry interaction. The flow field was found to be in excellent agreement with experimental data supporting the applicability of the solver with a dynamic subgrid turbulence model to highly swirling flows. Temperature and major species mass fraction profiles were generally well predicted demonstrating the capabilities of the subgrid PDF approach. Similar to previous numerical studies of this particular combustor, heat loss in the experiments was found to be the source of local temperature overestimation towards the combustion chamber walls. The implementation of non-adiabatic walls can thus be identified as a potential scope of ensuing work. Furthermore it has to be noted, that both the flame length and width were slightly under predicted - corresponding to faster combustion - compared to experimental measurements. This may be attributed to the utilisation of only one stochastic field in the calculation of the subgrid PDF evolution equation. Subsequent simulations with a larger number of stochastic fields will show if further improvement of the results can be achieved. In order to analyse the computed instantaneous thermochemical properties, an additional simulation using four stochastic fields was performed providing satisfactory agreement with measurement data. In summary, the employed LES method has been validated for partially premixed combustion in a complex geometry. All results were obtained without any adjustments to the model constants underlining the method's robustness in the simulation of turbulent reacting flow problems. A future extension of the method to fully compressible flow may reproduce thermo-acoustic instabilities observed in the experiments.

Acknowledgements

The authors are grateful to SIEMENS Industrial Turbomachinery Ltd. for their financial support. This work used the ARCHER UK National Supercomputing Service (http://www.archer.ac.uk).

References

[1] Pitsch, H., "Large-Eddy Simulation of Turbulent Combustion", *Annu. Rev. Fluid Mech.* 38:453–482 (2006).

[2] Jones, W.P., Navarro-Martinez, S., "Large eddy simulation of autoignition with a subgrid probability density function method", *Combust. Flame* 150:170–187 (2007).

[3] Jones, W.P., Prasad, V.N., "Large Eddy Simulation of the Sandia Flame Series (D-F) using the Eulerian stochastic field method", *Combust. Flame* 157:1621–1636 (2010).

[4] Jones, W.P., Prasad, V.N., "LES-pdf simulation of a spark ignited turbulent methane jet", *Proc. Combust. Inst.* 33:1355–1363 (2011).

[5] Brauner, T., Jones, W.P., Marquis, A.J., "LES of the Cambridge Stratified Swirl Burner using a Sub-grid pdf Approach", *Flow, Turbul. Combust.* 96:965–985 (2016).

[6] Jones, W.P., Marquis, A.J., Noh, D., "LES of a methanol spray flame with a stochastic sub-grid model", *Proc. Combust. Inst.* 35:1685–1691 (2015).

[7] Gallot-Lavallée, S., Jones, W.P., "Large Eddy Simulation of Spray Auto-ignition under EGR Conditions", *Flow, Turbul. Combust.* 96:513–534 (2016).

[8] Bulat, G., Jones, W.P., Marquis, A.J., "Large Eddy Simulation of an industrial gas-turbine combustion chamber using the sub-grid PDF method", *Proc. Combust. Inst.* 34:3155–3164 (2013).

[9] Bulat, G., Jones, W.P., Marquis, A.J., "NO and CO formation in an industrial gas-turbine combustion chamber using LES with the Eulerian sub-grid PDF method", *Combust. Flame* 161:1804–1825 (2014).
[10] Meier, W., Weigand, P., Duan, X.R., Giezendanner-Thoben, R., "Detailed characterization of the dynamics of thermoacoustic pulsations in a lean premixed swirl flame", *Combust. Flame* 150:2–26 (2007).
[11] Roux, S., Lartigue, G., Poinsot, T., Meier, U., Bérat, C., "Studies of mean and unsteady flow in a swirled combustor using experiments, acoustic analysis, and large eddy simulations", *Combust. Flame* 141:40–54 (2005).
[12] Galpin, J., Naudin, A., Vervisch, L., Angelberger, C., Colin, O., Domingo, P., "Large-eddy simulation of a fuel-lean premixed turbulent swirl-burner", *Combust. Flame* 155:247–266 (2008).
[13] Moureau, V., Domingo, P., Vervisch, L., "From Large-Eddy Simulation to Direct Numerical Simulation of a lean premixed swirl flame: Filtered laminar flame-PDF modeling", *Combust. Flame* 158:1340–1357 (2011).
[14] Franzelli, B., Riber, E., Gicquel, L.Y.M., Poinsot, T., "Large Eddy Simulation of combustion instabilities in a lean partially premixed swirled flame", *Combust. Flame* 159:621–637 (2012).
[15] Wang, P., Froehlich, J., Maas, U., He, Z., Wang, C., "A detailed comparison of two subgrid scale combustion models via large eddy simulation of the PRECCINSTA gas turbine model combustor", *Combust. Flame* 164:329–345 (2016).
[16] Volpiani, P.S., Schmitt, T., Veynante, D., "Large eddy simulation of a turbulent swirling premixed flame coupling the TFLES model with a dynamic wrinkling formulation", *Combust. Flame* 180:124–135 (2017).
[17] Smagorinsky, J., "General Circulation Experiments With the Primitive Equations", *Mon. Weather Rev.* 91:99–164 (1963).
[18] Piomelli, U., Liu, J., "Large-eddy simulation of rotating channel flows using a localized dynamic model", *Phys. Fluids* 7:839–848 (1995).
[19] Schmidt, H., Schumann, U., "Coherent structure of the convective boundary layer derived from large-eddy simulations", *J. Fluid Mech.* 200:511–562 (1989).
[20] Gao, F., O'Brien, E.E., "A large-eddy simulation scheme for turbulent reacting flows", *Phys. Fluids A* 5:1282–1284 (1993).
[21] Dopazo, C., O'Brien, E.E., "Functional formulation of nonisothermal turbulent reactive flows", *Phys. Fluids* 17:1968–1975 (1974).
[22] Valiño, L., "A Field Monte Carlo formulation for calculating the probability density function of a single scalar in a turbulent flow", *Flow, Turbul. Combust.* 60:157–172 (1998).
[23] Sabel'nikov, V., Soulard, O., "Rapidly decorrelating velocity-field model as a tool for solving one-point Fokker-Planck equations for probability density functions of turbulent reactive scalars", *Phys. Rev. E* 72:1–22 (2005).
[24] Mustata, R., Valiño, L., Jiménez, C., Jones, W.P., Bondi, S., "A probability density function Eulerian Monte Carlo field method for large eddy simulations: Application to a turbulent piloted methane/air diffusion flame (Sandia D)", *Combust. Flame* 145:88–104 (2006).
[25] Barlow, R.S., Karpetis, A.N., Frank, J.H., Chen, J.Y., "Scalar profiles and NO formation in laminar opposed-flow partially premixed methane/air flames", *Combust. Flame* 127:2102–2118 (2001).
[26] Sung, C.J., Law, C.K., Chen, J.Y., "Augmented reduced mechanisms for NO emission in methane oxidation", *Combust. Flame* 125:906–919 (2001).